

## Elimination of spatiotemporal disorder by Fourier space techniques

G. K. Harkness, G.-L. Oppo, R. Martin, A. J. Scroggie, and W. J. Firth

*Department of Physics and Applied Physics, University of Strathclyde, Glasgow G4 0NG, Scotland*

(Received 26 March 1997; revised manuscript received 25 March 1998)

A recently proposed method for the stabilization of unstable patterns uses an instantaneous feedback derived from the Fourier transform of the output [R. Martin *et al.*, Phys. Rev. Lett. **66**, 4007 (1996)]. We successfully extend this method to regimes of spatiotemporal disorder. By focusing on two different nonlinear optical systems, a laser and a Kerr slice with feedback, we demonstrate the usefulness, effectiveness, and generality of the technique. Our method allows for high power outputs without loss of spatial and temporal coherence. It also provides the possibility of pattern selection and, in some instances, tracking within a disordered regime. [S1050-2947(98)11209-X]

PACS number(s): 42.65.Sf, 47.54.+r

### I. INTRODUCTION

The coupling of spatial and temporal degrees of freedom in nonlinear dynamical systems often leads to loss of spatiotemporal coherence. A simple suppression of such behavior can be obtained by reducing either the nonlinearity or the number of spatial degrees of freedom (as in the use of apertures in laser cavities). Such approaches always result in serious limitations for practical applications. A less restrictive restoration of spatial and temporal order is a highly desirable feature in fields as diverse as laser and plasma physics as well as hydrodynamics.

Several techniques have recently been proposed to suppress spatiotemporal disorder in systems governed by partial differential equations [1–8]. One such approach has been to decompose the system onto a small number of spatial modes and then to apply the standard techniques of temporal control [9–11] to the resulting low-dimensional system [1,2,4,8]. Other methods require complicated mathematical transformations, which makes them difficult to implement in experimental systems with fast dynamics [2,3,5]. Finally, specific techniques have been successfully developed for particular types of instability or spatiotemporal structure [3,6].

The stabilization method we recently introduced [12] is based on feedback of spatial information filtered in Fourier space and is particularly amenable to application in optics. This is because, in an optical system, it is easy to obtain the spatial Fourier transform (or far-field) by using a single lens; the control technique can then be implemented in a fully optical manner [13]. In [12] we focused on the use of such a technique to stabilize, select, and track unstable patterns. The usefulness of filtering in Fourier space for control purposes has also recently been discussed in conjunction with optical delay for one-dimensional models of semiconductor lasers [14]. It is important to stress that the method introduced in [12] and applied here uses no delay since the feedback time is several orders of magnitude faster than the characteristic time scale of our mean-field dynamics and the feedback is coherent with the optical field. Note also that the absence of delay simplifies application to experiments and numerical simulations.

In this paper, we describe the extension of the Fourier space technique introduced in [12] to the elimination of spa-

tiotemporal disorder, and discuss the feasibility of such experiments in nonlinear optics. To this end, we will discuss the application of our control method to two specific optical models that display pattern formation and optical turbulence: a Kerr slice with feedback mirror [15–17] and a broad-area laser [18,19]. These systems display spatiotemporal disorder induced by instabilities of a different nature, as will be explained later. The successful elimination of spatial and temporal disorder for a wide range of parameter values in both systems is an indicator of the generality of our method.

### II. ELIMINATION OF DISORDER IN A LIQUID CRYSTAL LIGHT VALVE MODEL

Our first example is a variant of a model describing a Kerr slice with feedback mirror, as introduced in Ref. [15], and later realized in many experiments [20–23]. In many of these realizations the Kerr nonlinearity is synthesized with a liquid-crystal light valve (LCLV) with a feedback signal. Such a system was originally introduced by Akhmanov *et al.* [24]; for a discussion of the LCLV device and its relation to the Kerr slice configuration, see [25]. The LCLV is a hybrid electrical/optical device that allows the phase shift of a “read” beam to be controlled by the intensity of a “write” beam. This phase shifted input field is fed back so as to fall on the “write” side of the LCLV after some distance of free space propagation. The loop also contains an output coupler of reflectivity  $R_0$ . Figure 1 shows details of the setup. For this system, the model equations [16,17] can be written as

$$-\left(\frac{\partial^2}{\partial x^2} + \frac{\partial^2}{\partial y^2}\right)n + \frac{\partial n}{\partial t} + n = |B|^2, \quad (1)$$

where  $B(x,y)$ , the backward field incident on the “write” side of the LCLV, is related to the input optical field,  $F(x,y)$ , through the relation

$$B(x,y,t) = \sqrt{R_0} \exp\left(i\sigma \frac{\partial^2}{\partial x^2} + i\sigma \frac{\partial^2}{\partial y^2}\right) F \exp(i\chi n). \quad (2)$$

The variable  $n(x,y)$  is the excitation of the simulated Kerr medium;  $\chi$  measures the strength of the phase modulation and  $\sigma$  measures the relative strengths of field diffraction and

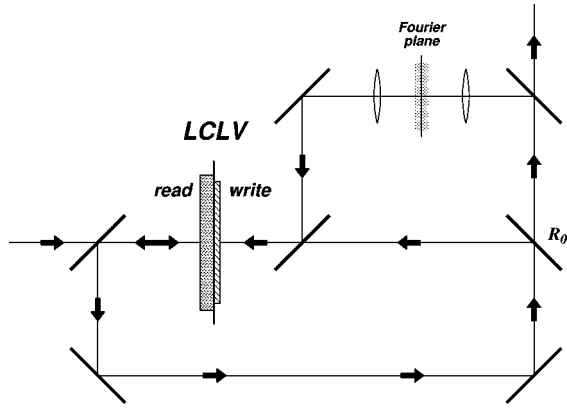


FIG. 1. A schematic diagram showing the control scheme we propose for the LCLV with feedback system.

diffusion of the medium excitation. The time variable  $t$  has been normalized to the LCLV reaction time, which is typically in the range of tens of milliseconds or longer. The spatial variables  $(x, y)$  have been normalized to the LCLV diffusion length, which in real systems is around 50 to 100  $\mu\text{m}$  [23].

For the LCLV system we consider a plane wave input field  $F = \sqrt{I}$  that describes the central part of the broad area beams used in such experiments [23]. For input intensities above some threshold, the plane wave output beam loses stability and forms a hexagonal pattern. For larger values of  $I$ , the hexagonal pattern breaks into fluctuating spots of light [17]. In the case of strong diffusion, this instability leads to “turbulent” motion shown in Fig. 2. The Fourier transform, averaged over several hundred units of time [Fig. 3(a)], clearly shows a large number of excited wave vectors. Such disorder strongly reduces spatial correlations, which decrease to around a tenth of the system size in the “turbulent” regime, as shown in Fig. 3(b). The spatiotemporal correlation of the output intensity  $I$  shown in Fig. 3(b) is defined by

$$C(r) = \langle \langle \langle I(\mathbf{x}', t) I(\mathbf{x}, t) \rangle_{\mathbf{x}} - \langle I^2(\mathbf{x}, t) \rangle_{\mathbf{x}} \rangle_t \rangle_{\phi}, \quad (3)$$

where  $(r, \phi)$  are the polar coordinates of the two-dimensional vector  $\mathbf{x} - \mathbf{x}'$ , and  $\langle \dots \rangle_{\alpha}$  indicates an average over the quantity  $\alpha$ . The power spectrum of the light inten-

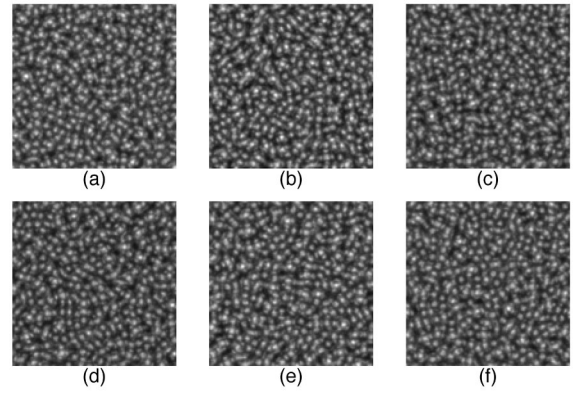


FIG. 2. Snapshots in time of the complex dynamics of the variable  $n$  in the LCLV model. Parameters are  $\sigma = 1$ ,  $\chi = 1$ ,  $I = 5$ ,  $R_0 = 0.9$ . Integrations were performed on a square grid of  $128 \times 128$  points with periodic boundary conditions. Black in the image denotes a small excitation and white a high one.

sity sampled locally is broadband, as shown in Fig. 3(c). All of these quantities quantify the degree of disorder of the system.

We can inhibit this spatiotemporal disorder by a number of equivalent approaches based on the Fourier technique of Ref. [12]. First, an additional feedback loop can be included into the LCLV setup, as shown in Fig. 1. By a similar mechanism to that described in our previous paper [12], a fraction of the field propagating to the “write” side of the LCLV is extracted and filtered in Fourier space to be recombined with the backward field. This corresponds to the addition, on the right-hand side of Eq. (2), of a control term [12] leading to

$$B_{\text{new}}(x, y, t) = [1 - s \mathcal{F}^{-1} M(k_x, k_y) \mathcal{F}] B(x, y, t), \quad (4)$$

where  $s$  is the strength of the control signal (its negative sign corresponding to increased losses of the controlled modes),  $\mathcal{F}$  is the Fourier transformation, and  $M(k_x, k_y)$  is the applied filter in the Fourier plane.

One important question regards the effect of the time delay induced by the additional control loop as, for example, discussed in [14]. For a typical feedback length of around 50 cm [23], the time delay is around a few nanoseconds while

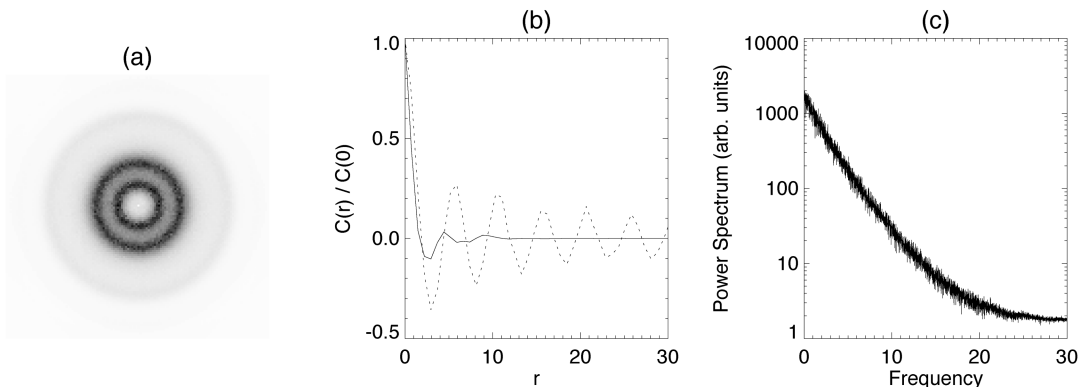


FIG. 3. Characterization of the dynamics of the LCLV model. The time-averaged Fourier transform intensity (far-field) is shown in panel (a). Intensity correlation functions, defined in the text, are shown in panel (b) for the “turbulent” dynamics (full line) and a stable hexagonal pattern, (dotted line). The locally sampled temporal power spectrum is shown in panel (c).

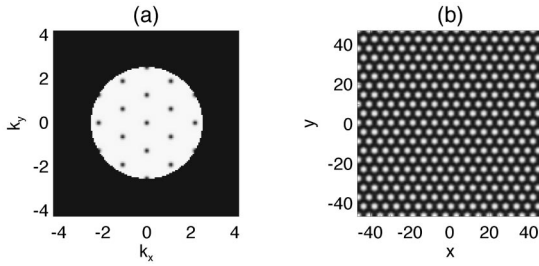


FIG. 4. (a) The mask shape  $M(k_x, k_y)$  used to control hexagons. Black indicates a value of zero and white a value of one. (b) A controlled hexagonal pattern. Parameters are the same as for Fig. 2 and a strength parameter  $s=0.3$  has been used.

the time scale of the LCLV system is at least seven orders of magnitude slower. Then, the control feedback can and should be considered instantaneous.

A further justification for introducing the control terms in Eq. (2) in the way we do is that our instantaneous feedback control (IFC) can be optically implemented in several different, but equivalent ways. For example, IFC can be obtained by placing a neutral density filter (NDF) at a Fourier plane in the original feedback loop. Note that Fourier filtering of LCLV systems has already been suggested as a technique for the correction of input phase distortions [26]. Our approach differs in that we stabilize unstable states of the system and that the effect of our filtering vanishes when order is achieved — our technique is noninvasive.

In the simulations we model the control by a mirror whose reflectivity depends on the incident wave vector  $\mathbf{k}$ ; the effective reflectivity is given by the formula

$$R(k_x, k_y) = R_0 [1 - sM(k_x, k_y)]^2,$$

where  $s$  gives the strength of the control and  $M(k_x, k_y)$  is the shape of the mask in Fourier space, normalized between zero and one. Using this or the NDF approach can simplify the experimental realization of the control technique. It is, however, not as flexible as the extra feedback loop approach where it is easier to change the value of  $s$  and to include rotations and phase manipulations as described in [12].

A typical mask shape used in Fourier space is shown in panel (a) of Fig. 4. The form of the mask is chosen based on the desired pattern, in this case a hexagonal pattern. The light corresponding to six wave vectors on a circle, and to their harmonics due to nonlinear mixing, is blocked, i.e.,  $M=0$  for dark regions of Fig. 4(a). The effect is to leave all wave vectors relevant to the desired pattern unaffected while undesired wave vectors will experience additional losses proportional to  $s$ .

In this way, we have been able to stabilize hexagonal patterns well beyond their normal regime of stability. Panel (b) of Fig. 4 shows this for the same parameters as in Fig. 2. As in Ref. [12], by suitable modification of the mask we have also successfully stabilized rolls and squares (see Fig. 5), exact but unstable solutions to this system. It is important to stress that our technique is noninvasive; the patterns it stabilizes are exact solutions of the original system without control. Visualized as a feedback, the control signal vanishes when control is established. As a quantitative measure of this fact, we compared the excitation,  $n$ , integrated over the

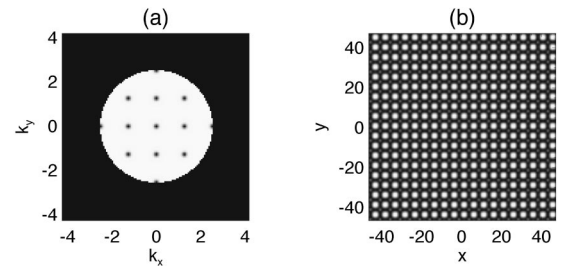


FIG. 5. (a) The mask shape  $M(k_x, k_y)$  used to control squares. Black indicates a value of zero and white a value of one. (b) A controlled square pattern. Parameters are the same as for Fig. 2 and a strength parameter  $s=0.3$  has been used.

transverse plane in the cases of “turbulent” and controlled dynamics. The controlled hexagonal pattern contains around 97% of the “energy” of the “turbulent” one.

As a further demonstration of the power of our method we have performed a tracking experiment with our model. The results are shown in Fig. 6. Panel (a) shows the time evolution of the maximum in space of the excitation density

$$n_{\max}(t) = \max_{(x,y)} n(x, y, t)$$

for the same parameters as in Fig. 2, that is, with input intensity  $I=5$ . The shaded area shows the range of this maximum and its width indicates the strength of the dynamical fluctuations. For a stable hexagonal pattern, there are no dynamics and so the shaded region is very narrow. In panel (b) the shaded area shows how these extrema of  $n_{\max}$  vary as a function of input intensity  $I$ . For  $I$  less than around 3.2, we obtain stable hexagons and above this we obtain dynamical (disordered) patterns.

In our tracking experiment, we start with input intensity  $I=5$ . Just as one might do in a real experiment, we study the time averaged far field, as shown in Fig. 3. We conclude that much of the energy in the turbulent regime is concentrated around wave vectors with modulus  $k \approx 1.2k_c$  where  $k_c$  is the wave vector of the patterns at threshold, which is around  $I=1.3$  for the chosen parameters. We construct a Fourier mask of hexagonal symmetry, as shown in Fig. 4, with a base size of  $1.2k_c$ . As already shown in Fig. 4, the application of such a mask can control a hexagonal pattern. The value of  $n_{\max}$  for the stabilized pattern is shown, as a diamond, at  $I=5$  in Fig. 6(b).

Keeping the same mask and strength, we now decrease the input intensity in order to track this solution. The other diamonds in panel (b) of Fig. 6 show the hexagonal solutions we have obtained. They are all exact solutions to the underlying system because the feedback signal vanishes. Note, however, in the figure that the stabilized solution and that of the uncontrolled system (dotted line) do not have the same threshold. We have, in fact, stabilized the exact hexagonal pattern based on a wave vector equal to  $1.2k_c$ , not  $k_c$ .

This further emphasizes the usefulness of our method. Not only can it be used to control disorder and to select between a number of different possible patterns [12], but it can also select between coexistent patterns of different wave vectors.

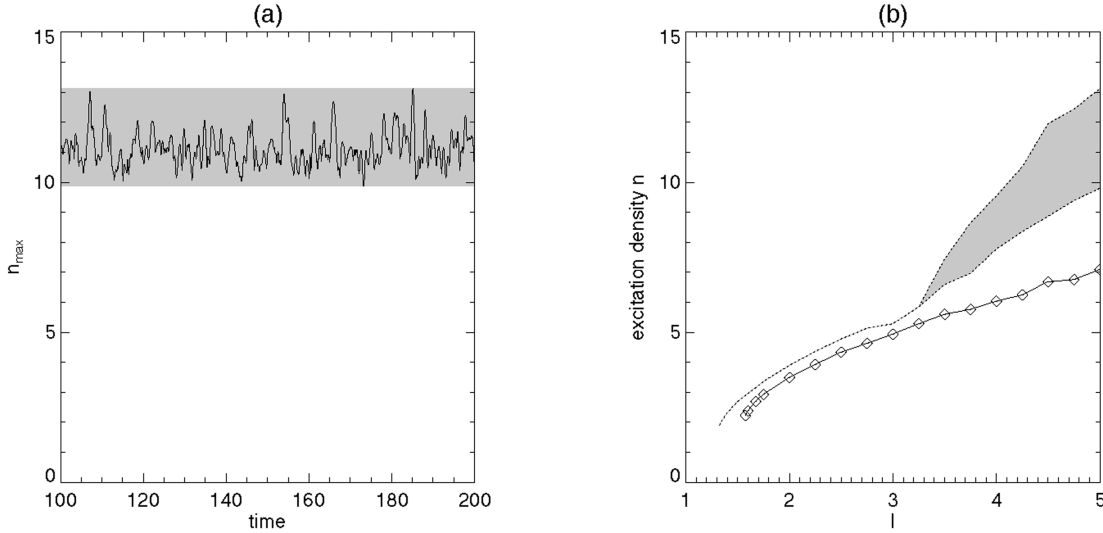


FIG. 6. (a) The maximum of the excitation density  $n(x,y)$  as a function of time. Parameters are the same as for Fig. 2. The shaded area shows the extrema. (b) The shaded area shows how the extrema plotted in (a) change as a function of the input intensity  $I$ . Diamonds show the maxima of the hexagonal patterns obtained by control, as described in the text.

### III. ELIMINATION OF DISORDER IN MODELS OF BROAD AREA LASERS

The second example configuration leading to spatiotemporal disorder is a broad area laser modeled by the mean field Maxwell-Bloch equations for the interaction of a laser field with a collection of two-level atoms [27]:

$$\begin{aligned} \frac{\partial F}{\partial t} &= -\kappa[(1-i\delta-i\nabla^2)F - P + sF_{\text{fb}}], \\ \frac{\partial P}{\partial t} &= -(1+i\delta)P + F\Delta, \\ \frac{\partial \Delta}{\partial t} &= -\gamma \left[ \Delta - \chi(x,y) + \frac{1}{2}(F^*P + FP^*) \right]. \end{aligned} \quad (5)$$

In these equations  $F(x,y,t)$  and  $P(x,y,t)$  are, respectively, the envelopes of the laser field and of the material polarization;  $\Delta(x,y,t)$  is the population inversion between the two atomic levels;  $(x,y)$  are the transverse coordinates normalized by the diffraction coefficient;  $\kappa$  and  $\gamma$  are, respectively, the damping rates of the electric field and of the population inversion, both scaled to the polarization damping rate;  $\delta$  is the detuning between the atomic and *mode-pulled* frequencies; and  $\chi(x,y)$  is a function describing the transverse variations of the input pump. The term  $sF_{\text{fb}}(x,y,t)$  describes the effect of our control method and will be discussed later.

For the case of a spatially homogeneous gain profile,  $\chi$ , and without control ( $s=0$ ) the system generates transverse traveling waves of the form [18]

$$F = f \exp(i\mathbf{k} \cdot \mathbf{r} - i\Omega t),$$

where  $\mathbf{k}$  and  $\Omega$  are related through the dispersion relation

$$\Omega = \frac{\kappa|\mathbf{k}|^2}{\kappa + 1}.$$

The critical wave vector  $|\mathbf{k}| = k_c$  is such that the laser operates at the atomic transition frequency in order to maximize  $|f|^2$ . Only the magnitude of the wave vector is selected by this mechanism, the direction of transverse propagation of the waves being entirely arbitrary.

We are interested here in the case of finite sized gain profiles in order to model real experiments. We consider a ‘‘top-hat’’ gain profile that is of a width equal to six times the most unstable wavelength. In other words, the width of the pump is equal to  $6 \times 2\pi/k_c$ . The main effect produced by this modification is to induce the appearance of sources and sinks of waves [28,19]. For certain ranges of parameter values, the source of waves can become unstable. This results in the erratic emission of ‘‘wiggles’’ in one transverse dimension and of ‘‘optical vortices’’ [29] in two dimensions, as shown in Figs. 7 and 8, for one and two transverse dimensions, respectively. These features are advected across the domain at the group velocity of the traveling waves [30]. By means of spatiotemporal correlations, such patterns have been shown to be weakly ‘‘turbulent’’ [31].

This instability can be suppressed by injecting into the laser an additional field  $sF_{\text{fb}}$ , derived from the output field  $F$  by filtering in Fourier space as shown in Fig. 9. The laser model (5) is based on the mean field approximation (suitable for solid-state, gas, vertical-cavity surface-emitting lasers, and high- $Q$  semiconductor lasers) where the round-trip time scale has been averaged out and the feedback control signal shown in Fig. 9 is instantaneous (IFC method). For short-pulsed, high gain, and very lossy lasers where the mean field approximation cannot be applied and model (5) loses validity, optical delay of the feedback signal has to be considered [14]. The resulting techniques are more difficult to implement both numerically and experimentally. Delay is not important for our IFC method, which, as for the LCLV case, can be equivalently described by the insertion of a neutral density mask at a Fourier plane in the cavity. We compute the feedback from

$$\hat{F}_{\text{fb}} = \hat{F}(k_x, k_y)M(k_x, k_y),$$

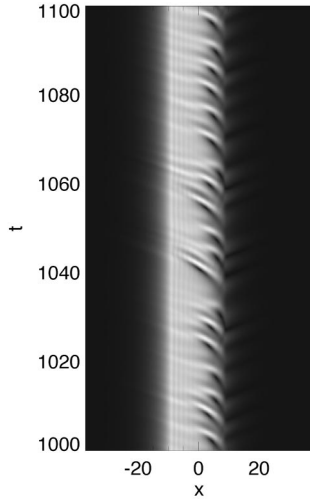


FIG. 7. Dynamics in a 1D two-level laser model. The one spatial dimension is plotted on the horizontal axis and time is plotted vertically. Black means a small value of the laser intensity and white means a large value. Parameters are  $\kappa = \gamma = 1$ ,  $\delta = 2$ , and  $\chi = 6$  with a top-hat profile of width 18.8. A series of “wiggles” are generated at a source on the right and propagate leftwards across the domain. We have used 256 transverse grid points with periodic transverse boundary conditions.

where the hatted variables are the Fourier transforms of the respective unhatted ones and  $M$  is the shape of the mask in Fourier space, again normalized between zero and one. The mask shape and feedback strength  $s$  are chosen so as to leave wave vectors within an annulus around  $k_c$  unaffected and to provide negative feedback for all other wave vectors. The instability in question arises due to the nonlinear coupling of a broadband of wave vectors around  $k_c$  and so the suppression of wave vectors away from  $k_c$  can control it.

This mechanism is identical to that used in the LCLV example but, due to the finite pump size, requires a further degree of care in its implementation. The finite pump size means that the resulting pattern cannot be made up of a small number of  $\delta$ -function Fourier modes, as for the cases considered in Ref. [12] and in the LCLV example. The resulting

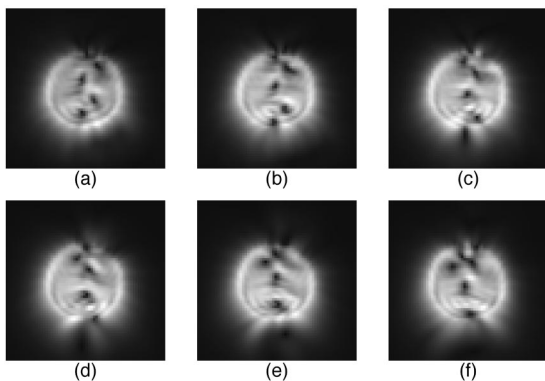


FIG. 8. Snapshots in time of the dynamics in a 2D two-level laser model. Black means a small value of the laser intensity and white means a large value. Parameters are  $\kappa = \gamma = 1$ ,  $\delta = 2$ , and  $\chi = 8$  with a circular top-hat profile of diameter 18.8. A series of “optical vortices” are generated erratically at a source near the top and propagate downwards.

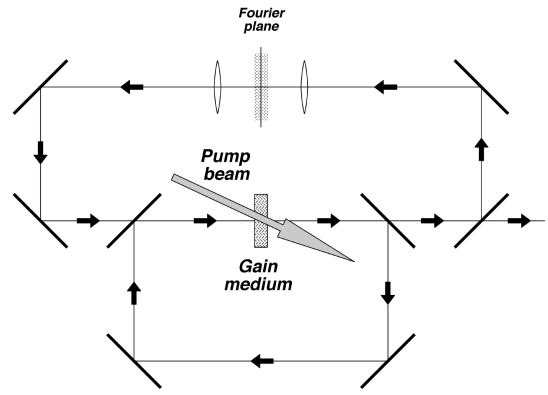


FIG. 9. A schematic diagram showing the control scheme we propose for the laser system.

far-field will approximately be a convolution between a pure pattern and the pump shape, giving the Fourier transform in the region of each wave vector of the pattern a finite width. We find that if the control annulus in  $k$  space is chosen to be too narrow, not allowing for this width, then the resulting controlled pattern is much broader than the uncontrolled one. However, if the annulus is chosen too broad, then the control scheme does not discriminate appropriately between wave vectors close to  $k_c$  and is ineffective. The choice of the feedback mask shape must therefore be a compromise between these two limits.

Typical feedback mask shapes for one- and two-dimensional geometries are shown in panels (b) and (e) of Fig. 10 and the resulting controlled states are shown in panels (c) and (f). Because of the finite size of the pattern we should not expect the feedback signal to vanish exactly when control is achieved, only to be small. In this case we compute

$$r = \frac{\int_T |sF_{fb}|^2 dA}{\int_T |F|^2 dA},$$

the ratio between the energy in the feedback field and in the laser field. The  $T$  in this expression denotes *the transverse plane*. For both the 1D and 2D cases shown, this quantity is less than 1%, indicating that the stabilized state is at least very close to an unstable state of the uncontrolled system. The power output of the controlled state is the same, within the bounds of numerical accuracy, as for the uncontrolled state. This further emphasizes the importance of this technique over more conventionally used “aperture” techniques discussed in the Introduction.

In order to assess just how close these stabilized solutions are to the unstable solutions of the original system, we must have a technique for finding these underlying solutions. It is this problem that we now consider.

### A. Stationary solutions

As discussed above, a laser of infinite transverse extent has exact traveling wave solutions [18]. In this case, one can study the effect of the control on these solutions and their stability. Such a study has been performed on the traveling

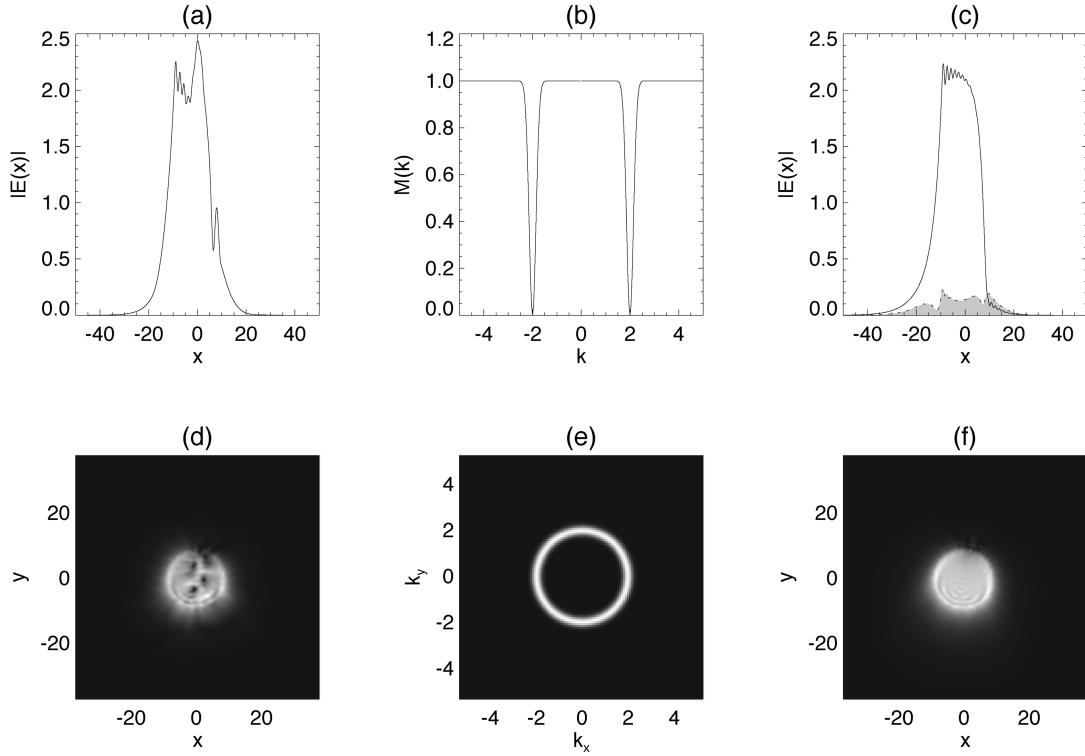


FIG. 10. Patterns from a laser model in 1D (upper) and 2D (lower) geometries. Panels (a) and (d) show the absolute value of the laser field as a function of the transverse coordinate(s). Parameters are  $\kappa = \gamma = 1$ ,  $\delta = 2$ , and  $\chi = 6$  in 1D and  $\chi = 8$  in 2D. Panels (b) and (e) show the feedback mask,  $M$ , used in the control, and panels (c) and (f) show the resulting states, controlled using a strength parameter  $s = 0.3$ . The shaded area in panel (c) shows the feedback signal  $|sF_{fb}|$  when control is achieved.

waves in a laser model enhanced to include some effects peculiar to semiconductor devices [14]. However, these exact solutions are not so relevant here for two main reasons. First, in a positively detuned two-level laser without transverse boundaries, independent of the parameters, there always exists an attracting, stable, traveling wave solution—so there is no complexity to control. Second, when the gain has a more realistic transverse profile, as in our case, these exact solutions no longer apply and the stability is radically altered. In this section, we describe a method we have used to find solutions relevant to the laser model with gain profile and to study their stability.

To make the problem more tractable we limit ourselves to one spatial dimension,  $x$ . We allow the pump to depend on space,  $\chi(x)$ , and look for solutions with the harmonic time dependence  $\exp(-i\Omega t)$ , solve the equations for the steady state values of  $P$  and  $\Delta$ , and insert these into the field equation to obtain

$$\left[ 1 - i\delta - i\Omega/\kappa - i\nabla^2 - \chi(x) \frac{1 - i(\delta - \Omega)}{1 + (\delta - \Omega)^2 + |f|^2} \right] f = 0, \quad (6)$$

where  $F(x, t) = f(x) \exp(-i\Omega t)$ . Note that if  $\chi$  is independent of  $x$ , then this equation has the same analytical traveling wave solutions as the original set (5). When this is not the case, we must resort to a numerical solution of Eq. (6). This method can yield all the stationary solutions,  $f(x)$ , not just the dynamically stable ones.

We discretize the transverse direction into  $N$  distinct points, reducing the original boundary value differential equation into a set of coupled, nonlinear, algebraic ones. We require to solve for  $N$  complex field values and the real frequency,  $\Omega$ , but because of the phase rotational symmetry of Eq. (6) we can take  $f(0)$  real. We assume periodic boundary conditions allowing us to compute the transverse Laplacian in Fourier space using a fast Fourier transform. This approach is more advantageous than a traditional low-order finite difference technique because its high accuracy,  $(dx)^N$ , allows us to use a smaller  $N$  for the same precision. We have also employed a technique that takes advantage of the fact that in regions where the pump  $\chi = 0$ , Eq. (6) is linear, with exponentially decaying traveling wave solutions

$$f \propto \exp(\lambda x),$$

with

$$\lambda^2 = -\Omega/\kappa - \delta - i.$$

The sign of  $\lambda$  is chosen so as to ensure an exponentially decaying field amplitude as  $|x| \rightarrow \infty$  and the constant of proportionality is chosen so that the solution matches onto the solution in a pumped region. Note that the phase waves always travel *outwards*.

With a top-hat pump profile  $\chi(x)$ , a typical stationary state is shown in Fig. 11. Panel (a) shows the field amplitude profile, stationary in time. Panel (b) shows a snapshot of the real part of the field. Due to the trivial time dependence

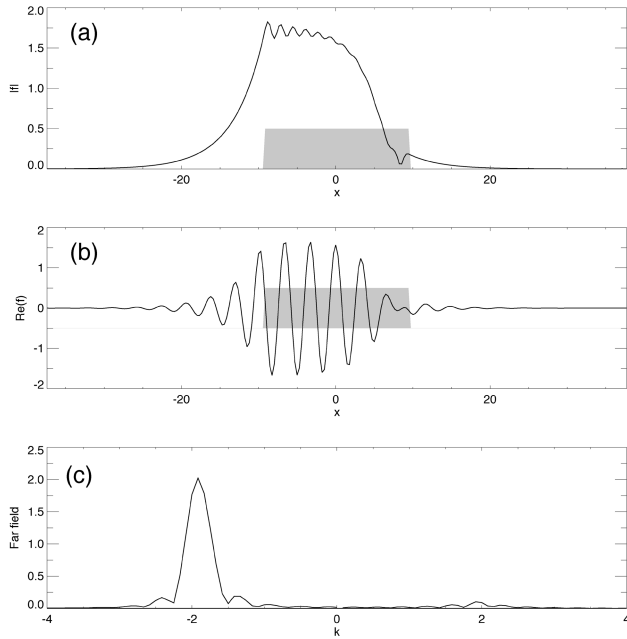


FIG. 11. A stationary solution to the laser equations. Panel (a) shows the absolute value of the laser field. The gray rectangle shows the extent of the pumped region. Panel (b) shows the real part of the laser field, emphasizing the traveling wave nature of the output. Panel (c) shows the Fourier transform (far-field) of the solution.

$e^{-i\Omega t}$  ( $\Omega \approx 1.84$  in this case), the waves propagate leftwards and rightwards away from the source at  $x \approx 10$ . Panel (c) shows the far-field (Fourier transform) of the solution. Note that it is strongly peaked near  $k \approx -2$ , indicating waves propagating mainly leftwards. The peak is, to a first approximation, the convolution of a  $\delta$  function, corresponding to a pure traveling wave, with the Fourier transform of the pump shape. Note also that there is a much smaller peak for positive  $k$  corresponding to waves propagating rightwards.

We already commented on this numerical method's ability to find both stable and unstable stationary solutions. A slight extension, detailed below, is able to determine their stability as well. We discretize the full set of Eqs. (5). We then find the eigenvalues of the matrix that results from linearizing around the stationary solution already found when solving Eq. (6). If any of these eigenvalues have a positive real part, then the solution is unstable.

As an example of the power of this method, we have tracked the solution shown in Fig. 11 over a range of pump values,  $\chi$ , computing its stability as we go. The results, in Fig. 12, show the frequency,  $\Omega$ , and the integrated intensity of that solution. A solid line indicates stable solutions, a dashed line unstable ones. The solutions' stability, established in this way, has been verified by direct numerical simulation of Eqs. (5). Close to threshold, there exist stable solutions that numerical simulations show to be globally attracting. For larger values of the pump, our stability analysis shows that these solutions become unstable via a Hopf bifurcation.

Further branches, representing a subset of the possible solutions, are shown in Fig. 13. These different branches correspond to solutions with different numbers of oscilla-

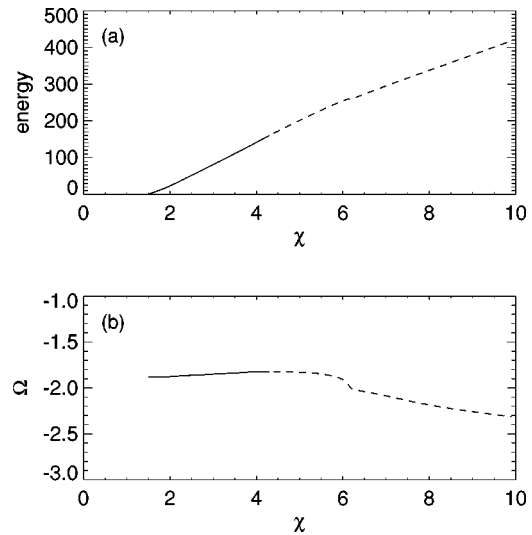


FIG. 12. The stability of the solution shown in Fig. 11, as a function of the pump parameter  $\chi$ . Panel (a) shows the space-integrated intensity of the laser field and panel (b) shows the solution's frequency,  $\Omega$ . The solution is stable only for values of  $\chi$  less than approximately 4.3 (solid line).

tions across the pumped region — see Fig. 11. At various points along these branches we have computed the stability of the solutions; unstable ones are shown as empty squares. The stable ones, shown as filled squares, constitute the Busse balloon [32]. All other branches we have found are unstable, independent of the value of  $\chi$ . Plotted as a dashed line on panel (ii) of Fig. 13 is the threshold for the various solutions. This is the equivalent of the *neutral stability curve* described in [32].

Figure 13 shows a number of interesting features. The solution (c), with the lowest threshold, the one shown in Fig. 11, is stable at threshold and its stability extends to more than twice the threshold value. Numerical simulations of Eqs. (5) starting from small amplitude noise show that it is this solution that is generally excited. Solutions with a value of  $\Omega$  close to that of solution (c), specifically (d) and (a), can also be stable but, in our experience, they are not usually excited in simulations that start from noise. Even at the places where the branches appear to bend back on themselves very sharply, they, and their derivatives, are in fact continuous. This phenomenon of solutions bending back on themselves is not found for pure traveling wave solutions in models with no gain profile. There is also no simple dispersion relation that assigns a particular transverse wave vector,  $k$ , to a solution with a given temporal frequency  $\Omega$ .

## B. Stabilization

Now that we have found and described the relevant stationary solutions, we can compare them to the solutions obtained when the control is switched on. Figure 14 shows the results of such a comparison. Two stationary solutions are shown: the one that has the lowest threshold, and the one that, far from threshold, has the largest output power. The diamonds show solutions stabilized by a feedback control using a mask designed to favor the solution with the lowest threshold. For small values of the pump, the stabilized solu-

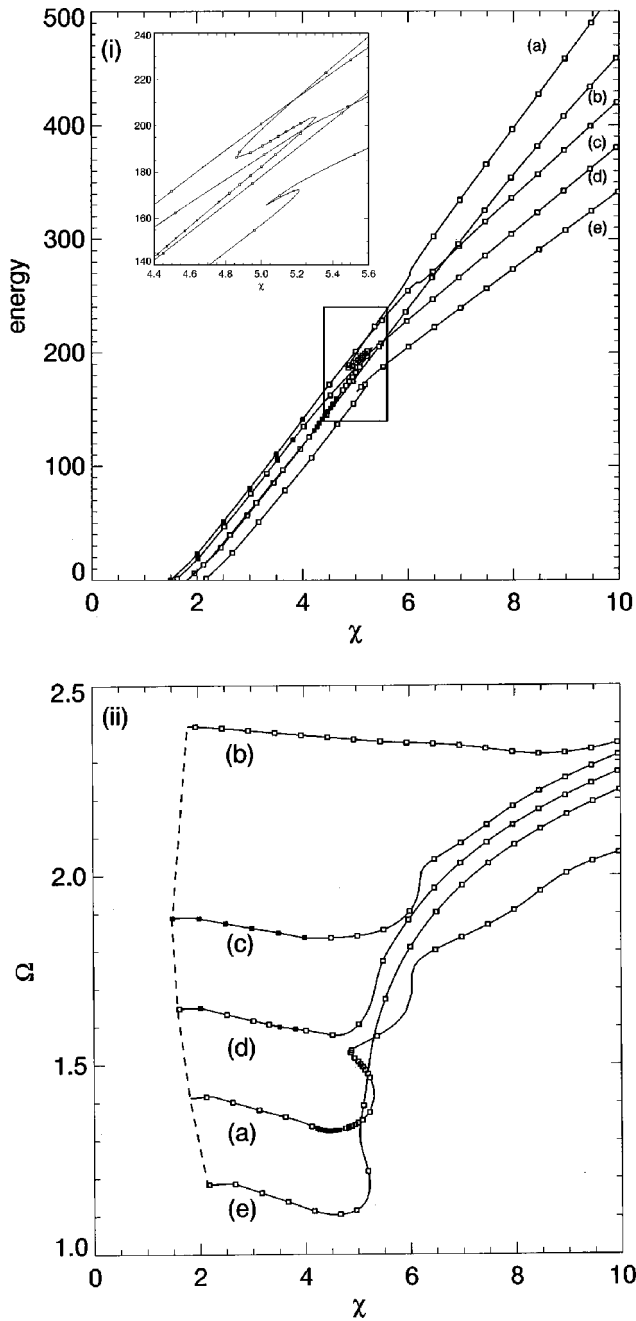


FIG. 13. A further subset of the possible solutions to the laser equations. Stability is indicated by filled squares, instability by empty ones. Panel (i) shows the space integrated intensity as a function of  $\chi$ , with the inset showing a magnification of the marked region. Panel (ii) shows frequencies  $\Omega$  associated with each solution branch. Also plotted, as a dashed line, is the threshold for each solution.

tion is very close to the stationary solution of the unperturbed system — the control is noninvasive. For larger values of the pump, although stabilization is achieved, the resulting state is not an exact stationary solution of the original system.

The origin of this discrepancy can be found by studying further the nature of the stationary solutions. Figure 15 shows the stationary solutions on the branch with lowest threshold for pump values  $\chi=3$  and  $\chi=8$ . Also plotted is

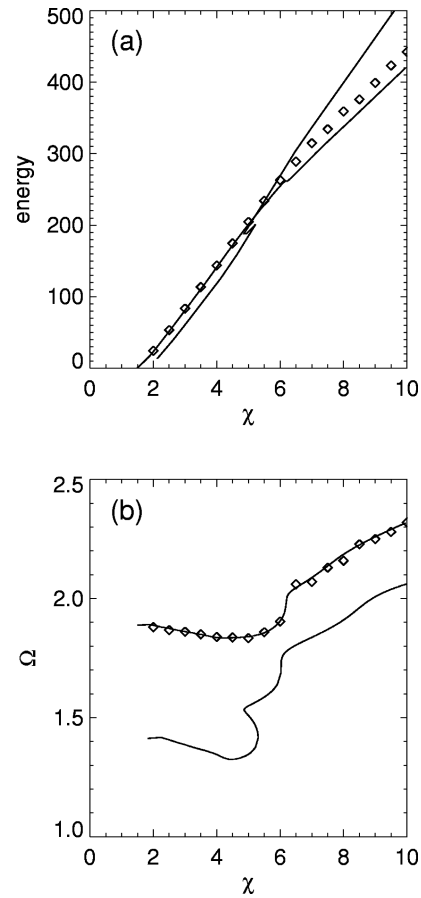


FIG. 14. A comparison between the solutions stabilized by our control method (diamonds) and those of the underlying system, plotted as full lines.

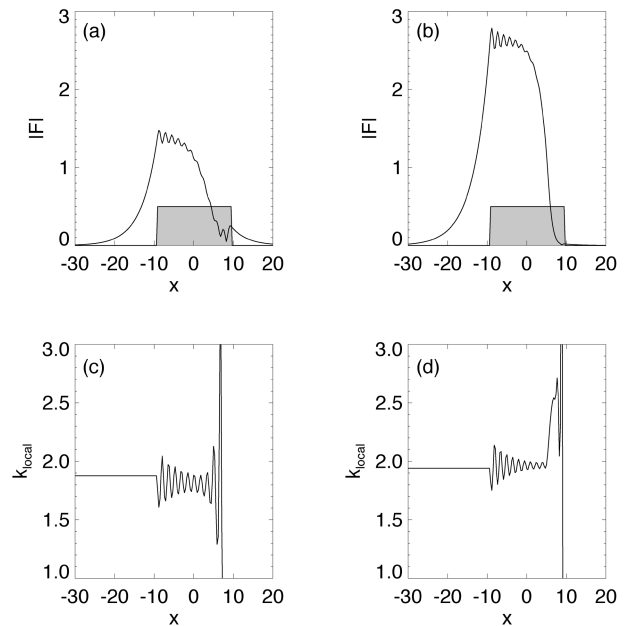


FIG. 15. Stationary solutions to the laser equations for  $\chi=3$  in panels (a) and (c) and for  $\chi=8$  in panels (b) and (d). Panels (c) and (d) show the local wave number  $k_{local}$ , defined in the text, as a function of the transverse coordinate  $x$ .

the local wave number defined as

$$k_{\text{local}}(x) = \text{Im} \left( \frac{\partial E / \partial x}{E} \right).$$

This is a useful definition because, if the field  $E \sim \exp(ikx)$ , then  $k_{\text{local}} = k$ . Note that to the left of the pumped region, because the field there is a pure (complex) exponential, the local wave vector is constant. To the right of the pumped region it is again flat with opposite sign compared to that on the left (not shown). For the case of  $\chi = 3$  the local wave vector in the pumped region shows small oscillations around an essentially constant value. These small oscillations are due to the fact that the field is not a pure leftward traveling wave but also has a small component of the rightward traveling wave.

For the solution at  $\chi = 8$ , there are the same small oscillations but the local wave number increases sharply at the right-hand side of the gain region, at the source of the traveling waves. This feature is common to all of the solutions we have found above around  $\chi = 6$ .

The IFC method relies on the target solution having essentially one transverse wave vector. Solutions that rely on a number of wave vectors for their precise shape cannot readily be stabilized. As we have shown above, this does not mean that a stable output cannot be achieved, just that the output obtained is not exactly a solution to the underlying system, an important distinction from a purist's point of view but not for applications. A high power, stable output can always be obtained from the laser with the application of the IFC technique.

#### IV. CONCLUSIONS

In conclusion, we have shown that by using carefully chosen instantaneous feedback constructed in the Fourier space, it is possible to stabilize complicated spatiotemporal behavior in pattern forming systems. Our technique is general, fast, and simple, not requiring expensive computation or interrogation of the system, and can be implemented in an all-optical way. We have demonstrated this in two different optical systems. For the case of periodic boundary conditions, the controlled states are exact, but unstable, solutions to the unperturbed system. With lateral boundaries, the stabilized solution is "close to" an unstable one of the original system.

Because of its simplicity and model independence, the technique shows great promise for use, both as a theoretical/computational tool to track unstable states into "turbulent" regimes and as an experimental tool to retain good spatial and temporal coherence for large values of the pump parameters. By extending this technique in combination with those proposed in Ref. [12], it is also possible to select between different pattern states in the disordered regime. For example, both squares and hexagons can be stabilized in a regime of optical turbulence in the LCLV system.

#### ACKNOWLEDGMENTS

We acknowledge EPSRC for financial support through Grant Nos. GR J/30998 and GR L/13636 and the British Council through Grant No. ARC 881. R.M. acknowledges the financial support of the EPSRC.

- 
- [1] H. Gang and H. Kaifen, *Phys. Rev. Lett.* **71**, 3794 (1993).
  - [2] F. Qin, E. E. Wolf, and H.-C. Chang, *Phys. Rev. Lett.* **72**, 1459 (1994).
  - [3] I. Aranson, H. Levine, and L. Tsimring, *Phys. Rev. Lett.* **72**, 2561 (1994).
  - [4] C. Lourenço, M. Hougardy, and A. Babloyantz, *Phys. Rev. E* **52**, 1528 (1995).
  - [5] V. Petrov, S. Metens, P. Borckmans, G. Dewel, and K. Showalter, *Phys. Rev. Lett.* **75**, 2895 (1995).
  - [6] A. Hagberg, E. Meron, I. Rubinstein, and B. Zaltzman, *Phys. Rev. Lett.* **76**, 427 (1996).
  - [7] W. Lu, D. Yu, and R. G. Harrison, *Phys. Rev. Lett.* **76**, 3316 (1996).
  - [8] R. Martin, A. J. Kent, G. D'Alessandro, and G. L. Oppo, *Opt. Commun.* **127**, 161 (1996).
  - [9] E. Ott, C. Grebogi, and J. A. Yorke, *Phys. Rev. Lett.* **64**, 1196 (1990).
  - [10] E. R. Hunt, *Phys. Rev. Lett.* **67**, 953 (1991).
  - [11] K. Pyragas, *Phys. Lett. A* **170**, 421 (1992).
  - [12] R. Martin, A. J. Scroggie, G.-L. Oppo, and W. J. Firth, *Phys. Rev. Lett.* **77**, 4007 (1996).
  - [13] R. Neubecker (private communication).
  - [14] M. E. Bleich, D. Hochheiser, J. V. Moloney, and J. E. S. Socolar, *Phys. Rev. E* **55**, 2119 (1997); D. Hochheiser, J. V. Moloney, and J. Lega, *Phys. Rev. A* **55**, R4011 (1997).
  - [15] W. J. Firth, *J. Mod. Opt.* **37**, 151 (1990).
  - [16] G. D'Alessandro and W. J. Firth, *Phys. Rev. Lett.* **66**, 2597 (1991).
  - [17] G. D'Alessandro and W. J. Firth, *Phys. Rev. A* **46**, 537 (1992).
  - [18] P. K. Jakobsen, J. V. Moloney, A. C. Newell, and R. Indik, *Phys. Rev. A* **45**, 8129 (1992).
  - [19] G. K. Harkness, W. J. Firth, J. B. Geddes, J. V. Moloney, and E. M. Wright, *Phys. Rev. A* **50**, 4310 (1994).
  - [20] M. Tamburrini, M. Bonavita, S. Wabnitz, and E. Santamato, *Opt. Lett.* **18**, 855 (1993).
  - [21] R. MacDonald and H. J. Eichler, *Opt. Commun.* **89**, 289 (1992).
  - [22] T. Honda, *Opt. Lett.* **18**, 598 (1993).
  - [23] R. Neubecker, G.-L. Oppo, B. Thuerling, and T. Tschudi, *Phys. Rev. A* **52**, 791 (1995).
  - [24] S. A. Akhmanov, M. A. Vorontsov, and V. Yu Ivanov, *Pis'ma Zh. Éksp. Teor. Fiz.* **47**, 611 (1988) [*JETP Lett.* **47**, 707 (1988)].
  - [25] *Self-Organization in Optical Systems and Applications in Information Technology*, edited by M. A. Vorontsov and W. B. Miller (Springer-Verlag, Berlin, 1995).
  - [26] M. A. Vorontsov and W. J. Firth, *J. Mod. Opt.* **40**, 1841 (1993).
  - [27] L. A. Lugiato and C. Oldano, *Phys. Rev. A* **37**, 3896 (1988).
  - [28] P. Couillet, T. Frisch, and F. Plaza, *Physica D* **62**, 75 (1993).

- [29] P. Coullet, L. Gil, and F. Rocca, *Opt. Commun.* **73**, 403 (1989).
- [30] G. K. Harkness, Ph.D. thesis, University of Strathclyde, Glasgow, U.K. (1994).
- [31] G. K. Harkness, J. Lega, and G.-L. Oppo, *Chaos Solitons Fractals* **4**, 1519 (1994); *Physica D* **96**, 26 (1996).
- [32] P. K. Jakobsen, J. Lega, Q. Feng, M. Staley, J. V. Moloney, and A. C. Newell, *Phys. Rev. A* **49**, 4189 (1994).